

Efficient Numerical Methods for Accurate Modeling of Soil Cutting Operations

A. Haeri^a, D. Tremblay^a, K. Skonieczny^a
D. Holz^b, M. Teichmann^b

^aDepartment of Electrical and Computer Engineering, Concordia University, Canada
^bCM Labs Simulations, Canada

^a{a_hae, kskoniec}@encs.concordia.ca, dominique.tremblay@concordia.ca, ^b{danielh, marek}@cm-labs.com

Abstract -

This research investigates the development and validation of state-of-the-art high-fidelity models of soil cutting operations. The accurate and efficient modeling of complex tool-soil interactions is an open problem in the literature. Modeling options that provide more flexibility in trading off accuracy and computational efficiency than current state-of-the-art continuum or discrete element methods are sought. In this work, two modern numerical methods, the material point method (MPM) and a hybrid approach, are presented with the goal to simulate excavation maneuvers efficiently and with high accuracy. MPM, as an accurate, continuum-based and meshfree method, uses a constitutive model (here, non-local granular fluidity model) for computing internal forces to update particle velocities and positions. The hybrid approach, a combination of particle and grid-based methods, avoids explicit integration scheme difficulties and unnecessary computations in the static regime. Visual and quantitative data, including forces on the excavation tool, are collected experimentally to evaluate these two simulation methods with respect to geometry of the soil deformation as well as interaction forces, both as a function of time.

Keywords -

Granular Flow; Physics-Based Simulation; Physically-Based Modeling; Terramechanics; Soil Mechanics; Computer Graphics; Experiment

1 Introduction

On Earth, construction, mining, and agricultural vehicles are extensively in contact with soil as a granular material. In space, exploration rovers are as well, as will robots for in situ resource utilization. However, granular flows and their interactions with rigid bodies are still poorly understood. In fact, their modeling is complex since they can experience various solid-like, fluid-like and gas-like deformations in time. Besides experiments, simulations can hugely contribute to this end. Nevertheless, the accurate and efficient modeling of complex tool-soil interactions is still an open research problem. In terms of accuracy, one

current direction of this research is the discrete element method (DEM), which simulates contact mechanics for millions of individual particles [1]. This state-of-the-art approach demonstrates promise in modeling but it is so computationally intensive as to be infeasible for real-time applications, and for large physical domains can be untenably expensive even in offline industrial applications [2]. On the other end of the complexity spectrum, several researchers highlight the insufficient predictive power of classical terramechanics models [3, 4], and their limitations to specific flow geometries [5], though they are computationally efficient.

In order to maintain a desired accuracy while enhancing computational efficiency, one possible direction is using methods from continuum mechanics. In continuum methods, there are two main aspects to make them appropriate for a specific modeling problem. One aspect is the constitutive model; it should be specific to the material being used to capture most of the static and/or flow regimes. For granular materials, they should generally cover elastic (solid-like), viscoplastic (fluid-like), and free (gas-like) behaviors. For the two extremes, elastic and free models have been developed based on soil mechanics (e.g. Drucker-Prager) and kinetic theory of gases, respectively. However, the middle regime of (visco) plastic deformation is more challenging. Plastic models can suffer from rate-independency [6] and in some cases, they may have issues with modeling strain hardening [7]. Whereas, viscoplastic models eliminate some numerical difficulties associated with plastic models, such as hardening [8]. In viscoplastic models, although local models [9] lack robustness in their ability to predict all flow phenomena, nonlocal models are accepted as highly predictive in different flow regimes [10]. The other aspect in continuum modeling is the numerical solver. Among the several continuum-based numerical solvers, finite difference (FD) for viscoplastic deformation, and finite element (FE) for elastic deformation, are the most common methods [11]. Both can yield good results in certain cases. However, the FD method has difficulties with extensional disconnection and static regime, while the FE method has issues when mesh dis-

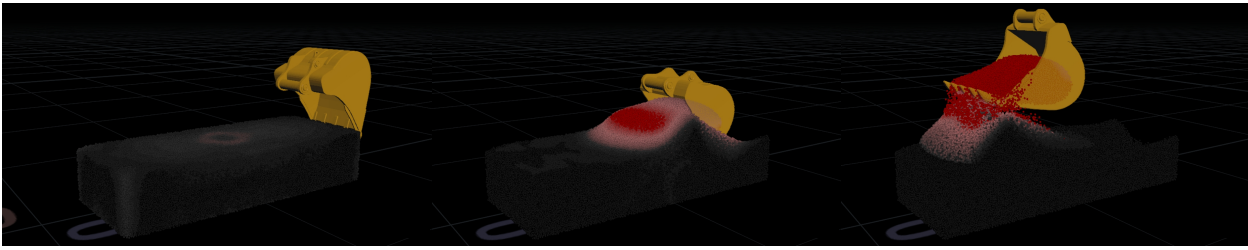


Figure 1. Industrial excavator modeling. Soil colors represent velocity magnitude.

tortion becomes large. Alternatively, the material point method (MPM) is a modern approach that combines the advantages of both FD and FE methods [12].

On the other hand, some novel techniques can be applied to terramechanics models to simultaneously maintain their efficiency and refine their accuracy and flexibility (i.e. extending to complex geometries). In fact, some intensive computations can be ignored in the physical domains that are in the static regime [13]. For the domains in the quasi-static regime which have less deformation, terramechanics models seem to be good candidates. With that, a classical terramechanics model is introduced by McKyes [14] as a method of trial wedges for 2-dimensional soil cutting (known as McKyes model). It is later generalized for 3-dimensional applications such as bucket of excavators and backhoes by Holz et al. [15]. In that, soil cutting forces are formulated based on the fundamental equation of earth-moving (FEE) [16]. Also, Skonieczny [17] replaces the generic surcharge force term in McKyes model with an explicit model of how cutting forces change due to accumulating soil. Thus, this model (McKyes) with all of its modifications can be employed for calculating forces on the cutting tool when the flow is quasi-static. Moreover, more flexible and advanced approaches can be applied to the domains in the intermediate regime specifically with (visco) plastic deformations. Particle-based methods are good candidates due to the nature of the granular flows. However, they often come with prohibitive computational cost, as in traditional DEM. An efficient granular material simulation method, based on Position Based Dynamics (PBD) Muller et al. [18], was introduced by Holz [19] as a faster variation of the traditional DEM. This method showed promising results and was experimentally verified in [20] for a wheel-on-soil configuration. Therefore, this parallel position based approach can be utilized to model the (visco) plastic granular flows when required, and even be used in combination with the modified McKyes model.

With the two aforementioned areas in mind, in this paper, two modern numerical methods are proposed for modeling of soil cutting. First, for the sake of accuracy, while being reasonably efficient, an efficient MPM (Moving Least Squares MPM) solver is utilized with an accurate constitutive model (nonlocal granular fluidity) developed

specifically for 3D MPM in a thermodynamically consistent manner and written in C++. Second, a real-time capable and relatively accurate hybrid simulation approach, combining particle and grid-based methods, is presented. This approach was previously introduced by Holz et al. [15] and is here extended with a dynamic soil failure angle calculation for soil cutting operations. Furthermore, the numerical results are compared and evaluated by the experimental data collected by innovative robotic equipment, designed for this type of operation.

2 Methodology

2.1 Numerical Methods

MPM with Nonlocal Granular Fluidity. As discussed, MPM is similar to the FE method but also takes the advantage of FD method by keeping an undeformed Cartesian background grid appropriate for large-deformation problems as well. In addition to the grid, MPM consists of particles that carry information (mass and momentum) during the simulation. The particles can freely deform and, at the end of each time step, transfer the information to the grid nodes and vice versa. The procedure of MPM with the nonlocal model is shown in algorithm 1.

The momentum equation ($\phi\rho\dot{v} = \phi\rho G + \text{div}T$) as the governing equation in the weak form

$$\frac{1}{\Delta t} \int_{\Omega} \phi\rho\Delta v q dV = \int_{\Omega} \phi\rho G q dV - \int_{\Omega} T\nabla q dV \quad (1)$$

is solved on grid nodes. Where v is velocity, T is Cauchy

Algorithm 1: MPM-NGF

1. Initialization
 - repeat**
 2. Articulate rigid bodies
 3. Calculate contact forces
 4. Affect gravity, internal and contact forces on particle
 5. Transfer momentum from particles to grid
 6. Solve momentum equation on grid nodes
 7. Calculate Laplacian term in NGF on grid
 8. Transfer momentum from grid to particles
 9. Advect particles and rigid bodies
 10. Calculate particle internal forces via NGF
 - until** *Simulation ends*;
-

stress tensor, G is gravity acceleration, ϕ is volume fraction, q is test function, ρ is density, and V is volume. The angular momentum and energy conservations are satisfied due to the symmetric stress tensor and the implementation of hyperelasticity framework, respectively. To discretize the spatial terms, the Moving Least Squares (MLS) shape function [21] is used. It can speed up MPM by eliminating the need for explicitly calculating the weighting function derivative. Furthermore, it is consistent with the APIC (affine particle-in-cell [22]) particle-grid transfer scheme in the sense that MLS-MPM uses the $\frac{\partial v}{\partial x}$ quantity from APIC, required in the deformation gradient update, to enhance efficiency.

One novel advance in this research is the accurate calculation of internal forces via the unsteady form of Nonlocal Granular Fluidity (NGF) model [23] with hyperelasticity. In fact, this is a thermodynamically consistent version of the nonlocal theory for three-dimensional MPM [24, 25]. Hyperelasticity requires keeping track of the deformation gradient, which is multiplicatively decomposed into elastic and plastic parts. The total deformation gradient is updated via $\dot{F} = \frac{\partial v}{\partial x} F$, and the elastic deformation gradient is calculated via $F^e = F(F^p)^{-1}$. The nonlocal constitutive model is hence utilized to calculate F^p . By assuming that the viscosity ($1/g$ where g is granular fluidity) is time-dependent, the unsteady PDE of the model

$$t_0 \frac{\partial g}{\partial t} = A^2 d^2 \nabla^2 g - (\mu_s - \mu)g - b \sqrt{\frac{\rho_s d^2}{p}} \mu g^2 \quad (2)$$

should be solved for granular fluidity g . Where t_0 is a constant time-scale, A is a dimensionless material parameter called nonlocal amplitude, and d , p , and ρ_s are grain diameter, mean normal stress and grain density, respectively. Also, b is a local rheology parameter, the friction coefficient μ , and static friction coefficient μ_s cause flow to happen. Then the equivalent plastic shear strain rate can be obtained via $\dot{\gamma}^p = g\mu$.

Since in MPM granular materials can be separated, the open-state particles should also be modeled. While kinetic theory of gases is capable of this modeling, in most cases it is accurate enough to handle granular gas via pure kinematics (stress-free). To detect this regime, pressure (mean normal stress) should be tracked for every individual particle. Figure 2 shows four possible states that can occur for a particle in the next time step.

The algorithm used to calculate the internal forces with the nonlocal model is inspired from [25] for the implementation of the hyperelasticity framework. It is well adapted for use in MPM with the techniques used to handle stress-free particles, and to solve the unsteady nonlocal equation explicitly (and uncoupled with the momentum equation). In this, the particle nonlocal Laplacian term is obtained via a second-order FD scheme on the centre grid node in

the kernel support of the particle, via equation (3) and the particle internal force can be obtained given the calculated Cauchy stress tensor.

$$\nabla^2 g_{i,j,k} = \frac{1}{\Delta x^2} (g_{i+1,j,k} + g_{i,j+1,k} + g_{i,j,k+1} - 6g_{i,j,k} + g_{i-1,j,k} + g_{i,j-1,k} + g_{i,j,k-1}). \quad (3)$$

The MPM code used is from Hu et al. [21] with an unsteady nonlocal model extension developed by authors of this paper, and written in C++. Also, two issues addressed as corner and penetration issues in [21] are fixed here. From a high performance computing (HPC) viewpoint, multithreading (via Intel TBB) and vectorization (via explicit SIMD) are utilized in the code, in addition to some algorithmic improvements. These techniques make the current MPM 2x faster than a traditional MPM [21].

Hybrid Approach. The hybrid approach presented in this work extends on the hybrid, particle- and grid-based simulation method introduced by Holz et al. [15], which is included in the dynamics simulation toolkit Vortex Studio, created by CM Labs Simulations Inc. In this simulation model, the static soil state is efficiently represented by a grid (a height field in this case). Soil portions in the grid that transition into a dynamic, moving state are replaced by particles. These so-called soil particles are simulated using the Parallel Particles solver (P^2) which ensures efficiency and unconditional stability [19]. The organization of soil in particles and grid is illustrated on the left side of Figure 3.

The motivation behind the described approach is to provide a computationally efficient and stable, yet accurate model, which, by modifying select discretization parameters such as particle count or simulation frequency, can achieve real-time or faster than real-time performance. By using only a limited number of particles at a time, namely the particles in motion, lower simulation frequen-

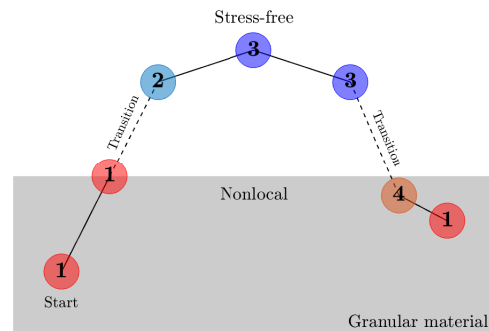


Figure 2. Possible states for a particle: under compression (red) and stress-free (blue). Gray area represents granular material.

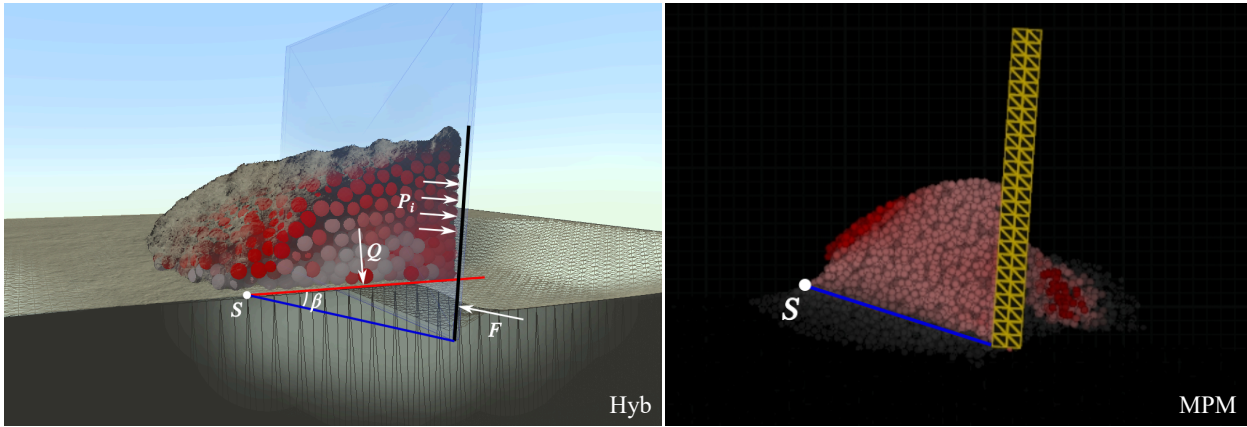


Figure 3. Left: Separation of simulated soil in particles and grid in the Hybrid method and force sources. Particle/blade contact forces, P_i , surcharge force, Q , applied to soil wedge, and McKyes cutting force, F , are indicated. Point S and angle β denote the soil failure point and the soil failure angle, respectively. Right: Soil deformation pattern in MPM method shows soil failure point S and linear soil failure surface.

cies, i.e., fewer steps per second, can be used without significantly reducing the solution accuracy or causing instabilities. This measure is a great tool for speeding up the proposed method up to real-time running times, as will be shown in Section 3.2.

In the aforementioned setting, soil reaction forces applied to the cutting blade are produced by two sources, the soil mass represented by particles, and the soil mass represented by the grid. Soil particles, which model the surcharge in front of the blade, directly exert contact forces to the contacting blade surface. And the soil grid applies force via a semi-empirical terramechanics model developed by McKyes [14]. This separation of forces is depicted in Figure 3. With increasing surcharge, i.e., increasing amount of soil particles, the soil reaction forces also increase. This is modeled by injecting a surcharge force into the McKyes model as described by Holz et al. [15] and explained in the following sections.

In the McKyes model, soil surface and blade are both assumed to be linear. A non-cohesive soil in front of a moving blade can then be assumed to fail along a straight line. This results in a triangular soil wedge formed by the surface of the terrain, the failure line and the blade. The forces acting on the soil wedge are depicted in Figure 4. In this configuration, the cutting force F per tool width required to induce soil failure and deform the soil can be computed as

$$F = \gamma g d^2 N_\gamma + c d N_c + Q N_Q + c_a d N_a \quad (4)$$

where

$$N_\gamma = \frac{(\cot \rho + \cot \beta) \sin(\alpha + \phi + \beta)}{2 \sin(\delta + \rho + \phi + \beta)}, \quad N_Q = \frac{\sin(\phi + \beta)}{\sin(\delta + \rho + \phi + \beta)}, \quad (5a)$$

$$N_c = \frac{\cos \phi}{\sin \beta \sin(\delta + \rho + \phi + \beta)}, \quad N_a = \frac{-\cos(\rho + \phi + \beta)}{\sin \rho \sin(\delta + \rho + \phi + \beta)} \quad (5b)$$

with gravity g , soil slope inclination angle α , tool/soil angle ρ , tool penetration depth d , soil failure angle β , soil internal friction angle ϕ , soil cohesion c , specific weight of the soil γ , tool/soil friction angle δ , tool/soil adhesion c_a and surcharge force per tool width Q .

In the original hybrid model [15], it was assumed that soil failure occurred in the passive Rankine state, leading to a constant soil failure angle β . However, it has been shown that the soil failure angle does not remain constant during a cutting operation and therefore must be dynamically updated [17]. We assume that for non-cohesive soils the point of failure (which is the intersection between soil surface and failure line) roughly occurs at the far end of the accumulating pile of soil that is being pushed by the blade. We verified this assumption in the context of our experiments based on visual inspection of soil failure patterns occurring in the experiments themselves, as well as by inspecting the particle flow in simulations obtained by MPM (cf. right side of Fig. 3). We make use of this assumption by walking across the particle skeleton in front of the blade and in the general blade's forward direction until no more particles can be visited. The position of the

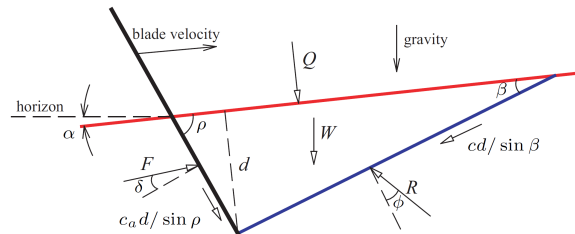


Figure 4. Forces acting on the soil wedge.

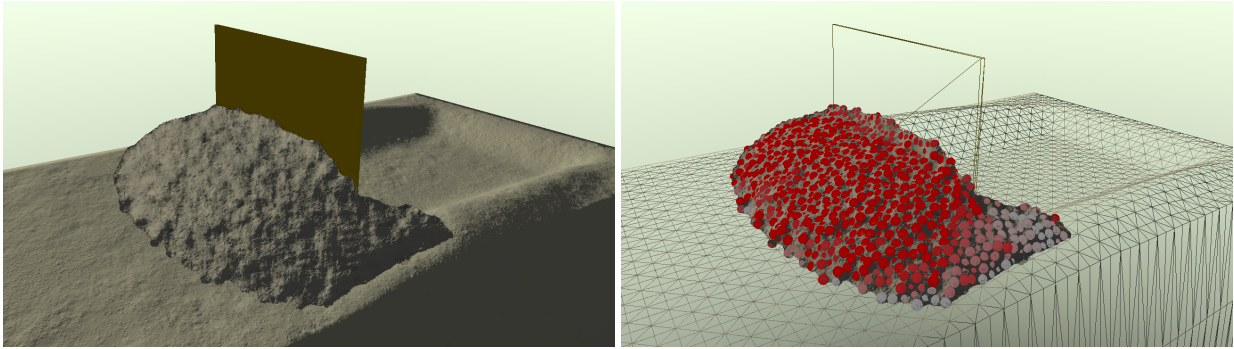


Figure 5. Hybrid method using real-time, screen-space visualization from [26] (left), and display of particles and grid (right), for experiment with 5-cm depth.

last visited particle indicates the location of the soil failure point and is used to compute the soil failure angle used in the McKyes model.

Once the soil failure point is found, the length of the soil wedge ahead of the blade can be determined. All particles sitting on top of this soil wedge contribute to the surcharge force Q from Equation 4, which is measured by summing up all contact forces of the particles colliding with the soil grid and sitting on top of the soil wedge. We experienced that introducing the full surcharge force into the McKyes model leads to too high a soil reaction force computed by the model. Consequently, we suggest a convenient force tuning parameter, denoted as *surcharge contribution factor* $s_q \in [0, 1]$, with which the surcharge force submitted to the McKyes model can be weighted, leading to the following modified version of Equation 4.

$$F = \gamma g d^2 N_\gamma + c d N_c + s_q Q N_Q + c_a d N_a \quad (6)$$

As will be shown in Section 3, the s_q -factor can be used to calibrate the hybrid method in order to match the simulated soil reaction forces to the forces that are observed in experiments.

2.2 Experimental Method

In this research, an excavation experiment (identical to the simulations) was set up to validate the numerical methods. It consists of a sandbox positioned under a 3-degree-of-freedom motorized unit to which an excavation accessory is attached. For this experiment and for the numerical simulation presented here, the excavation accessory is a flat plate (blade) as depicted in Figure 6 (top). The rake angle of the blade can be set manually and it remains constant during the run. The excavator can be moved horizontally and vertically independently. The motors are controlled such that the impulses from the soil flow do not affect the trajectory of the excavator. The excavator is installed on a force-torque sensor Delta IP60 (ATI Industrial Automation Inc.) that measures the forces

and torques on the blade along each direction. The blade trajectory is composed of three segments: first, a downward ramped motion at the start to dive into the soil with a specific depth, then a long-duration horizontal motion, and finally an upward ramp in the end to resemble the motion of an industrial excavator. Two tests were done based on this trajectory but at different (2-cm and 5-cm) depths.

The soil in the experiment is a NASA Glenn Research Center lunar soil simulant (GRC-1). The relative density used is 44.6 +/- 7.2%. This is calculated based on the cone index gradient of 5.30 +/- 0.6 kPa/mm using the correlation in [27]. Thus, the corresponding internal friction angle can be obtained as 35 deg. The grain diameter and density are 0.3 mm and 2583 kg/m³. Using the triaxial test performed by Oraveca et al. [27] the estimated Young's and shear moduli are 150 and 60 kPa, respectively. Also, the measured external friction angle between the blade and soil is ~30 deg. The setup of the experiment is shown in Figure 6.

3 Results

3.1 Experimental Verification

The tool-soil interactions in the simulations here are evaluated by the forces measured in the experiments (torque comparison is left). Figure 7 compares all the forces from the experiment, MPM and Hybrid method. The quantitative force values are in good agreement with the experimental forces in the three (forward, vertical and lateral) directions. A quantitative assessment of the simulation accuracy in terms of mean percentage error (MPE) is provided in Table 1. Due to the fast technique used to calculate the nonlocal Laplacian term in MPM, the MPM results seem to be slightly more oscillatory than the experimental results. However, in addition to the overall trend, MPM is able to capture drops and rises in force at various time steps of the two experiments. This can highlight the unsteady form of the MPM solver as well as the nonlocal constitutive model. Also, as a real-time method,

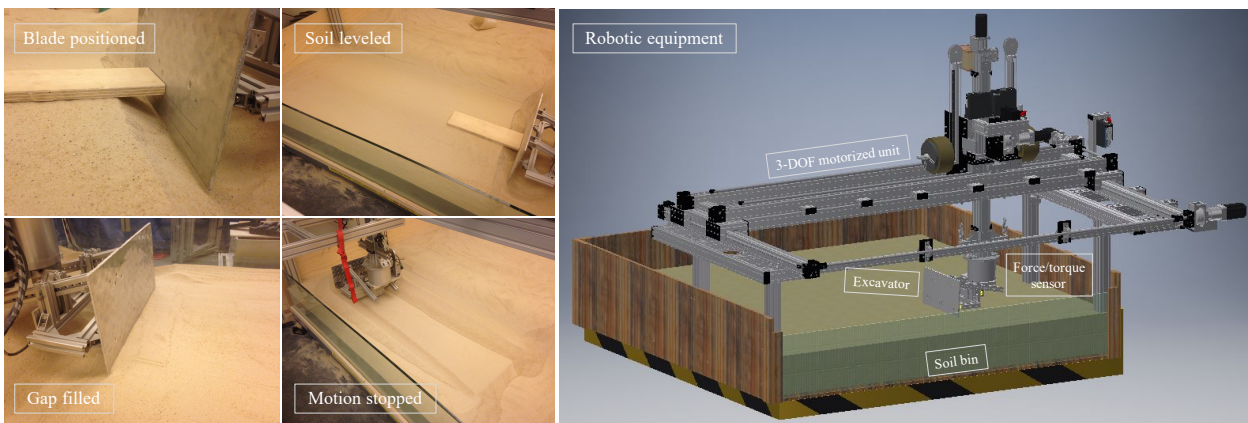


Figure 6. Robotic equipment and experiment setup.

Hybrid has the ability to predict forces as deformations increase. In fact, this time-dependent prediction is made possible by the introduction of the dynamic soil failure angle in the McKyes model, and modeling of the accumulating soil surcharge by particles. Note, that the surcharge contribution factor $s_q = 0.1$ was found to produce the best match between the Hybrid method and the experimental results. All other simulation parameters are set based on the physical properties of the soil used in the experiment.

A qualitative and visual comparison of the simulations and the experiment is shown in Figure 8. This illustration shows the soil geometry at the end of the second trajectory segment in the 5-cm experiment for both MPM and Hybrid method. Also, a real-time soil visualization for the 5-cm experiment simulated with the hybrid method is provided in Figure 5. In general, the soil behavior in MPM and Hybrid are predicted similar to the one in the experiment. The particle velocities visualized in colors clearly depict the static (gray) and dynamic (red) parts; while static parts in Hybrid are visualized as grid consistent with its methodology. The MPM velocity field is more compatible with the experiment. It can be due to either the nature of MPM as a continuum-based method or the higher number of particles used. However, even with a lower number of particles and with real-time running times, the Hybrid velocity field is still in good agreement with the experiment, as can also be seen in Figure 5.

3.2 Run-Time Measurements

We measured the computational time spent in both MPM and Hybrid method with 20 seconds of simulated time in the 5-cm depth excavating experiment. The measurements were performed on an Intel(R) Core(TM) i7-6700 CPU @ 3.40GHz with 4 physical cores for MPM, and on an Intel(R) Core(TM) i7-8700 CPU @ 3.20GHz with 6 physical cores for the Hybrid method. The results are provided in Table 1.

Run-time as well as accuracy of both methods can be influenced by modifying the simulation discretization parameters, e.g. particle count and simulation frequency. In order to demonstrate this fact, the mean percentage error (MPE) of the forward cutting force in the simulation relative to the experiment was calculated for different discretization settings.

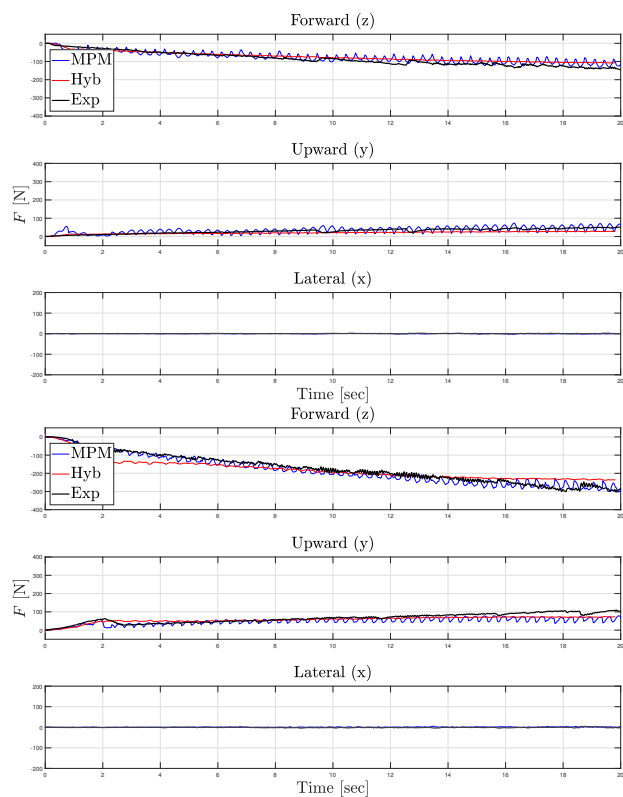


Figure 7. Interaction forces from MPM, Hybrid, and experiment for 2-cm (top) and 5-cm (bottom) depths.

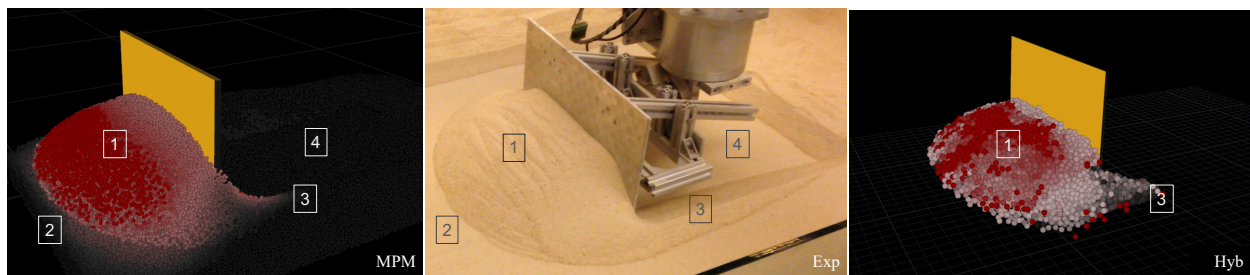


Figure 8. Geometries of soil deformations in MPM, Hybrid, and experiment for 5-cm depth. Four visual criteria are emphasized for comparison.

As can be seen in the results, MPM runs slower than real-time on the target hardware but can be substantially sped up by reducing the number of particles per cell (ppc) and/or increasing the grid spacing (Δx), both of which results in a lower particle count. Using a lower simulation frequency, i.e., a larger time step (Δt), would also lead to a simulation speed-up, but since in MPM equations are solved explicitly, the stability condition could become violated as a consequence. An implicit MPM solver could rectify this issue and would be future work.

The Hybrid method can run at real-time or faster than real-time by reducing particle radius and simulation frequency. Due to its implicit nature, the hybrid method remains stable regardless of the chosen simulation frequency. However, as can be seen in the results, the MPE increases significantly for simulation runs with lower simulation frequencies. This situation can be remedied by also choosing larger particle radii at which point the error reduces. This effect is likely due to excessive particle collisions or tunneling artifacts caused by particles being too small compared to the distances they travel between steps at low simulation frequencies. Thus, by choosing appropriate discretization settings, the error in the Hybrid method can be reduced to a level that rivals with the precision achieved in the MPM simulations with faster run-time settings.

4 Conclusion

Two efficient simulation methods for soil cutting operations have been presented and compared with experimental results. Both methods show good agreement with the experiments, with the MPM method yielding more accurate results than the Hybrid method. While the MPM method runs consistently slower than real-time, the Hybrid method can produce results at real-time and even faster than real-time without significant loss in accuracy. This ability makes the Hybrid method well-suited for use in virtual prototyping contexts such as the development of a real-time excavation automation control system. Accurate and efficient simulation methods are specifically useful in the

training of machine-learning algorithms since faster simulation allows accelerating the training procedure. For an example application in which a precursor of the presented Hybrid method has been used for design of an excavator automation system the reader is referred to [28].

References

- [1] C. Osullivan and J. Bray. Selecting a suitable time step for discrete element simulations that use the central difference time integration scheme. *Engineering Computations*, 2004.
- [2] S. Dunatunga and K. Kamrin. Continuum modeling of projectile impact and penetration in dry granular media. *J. Mech. Phys. Solids*, 100:45–60, 2017.
- [3] L. Ding, Z. Deng, H. Gao, J. Tao, K. Iagnemma, and G. Liu. Interaction mechanics model for rigid driving wheels of planetary rovers moving on sandy terrain with consideration of multiple physical effects. *Journal of Field Robotics*. In press., 2014.
- [4] C. Senatore and K. Iagnemma. Analysis of stress distributions under lightweight wheeled vehicles. *Journal of Terramechanics*, 51:1–17, 2014.
- [5] J. Shen and R. Kushwaha. *Soil-machine interactions: a finite element perspective*. Books in soils, plants, and the environment, 1998.
- [6] W. Chen and G. Baladi. Soil plasticity: Theory and implementation. 1985.
- [7] G. Klar, T. Gast, A. Pradhana, C. Fu, C. Schroeder, C. Jiang, and J. Teran. Drucker-prager elastoplasticity for sand animation. *ACM Transactions on Graphics*, 2018.
- [8] W. Abdullah. Viscoplastic finite element analysis of complex geotechnical problems. *Journal of Civil Engineering*, 5, 2011.
- [9] P. Jop, Y. Forterre, and O. Pouliquen. A constitutive law for dense granular flows. *Letters*, 441, 2006.

Table 1. Method comparison for 20-sec simulation of 5-cm depth experiment. Number of steps as well as average run-time per simulated second of the experiment are provided. The *-symbol in the *Method* column indicates real-time or faster than real-time performance. The column *Discretization* provides grid spacing and particle radius values utilized in simulations by the MPM and the Hybrid method, respectively. Mean percentage error (MPE) in forward force is specified relative to the experiment.

Method	# Steps/sec	Discretization	Particle # (ppc)	Total Run-Time	Avg Run-Time/sec	Error (MPE)
MPM	10K	0.0033 m	230K (8)	8.0K sec	400 sec	-9.9%
MPM	10K	0.0033 m	32K (1)	1.5K sec	75 sec	-14.8%
MPM	3K	0.0040 m	15K (1)	220 sec	11 sec	15.8%
Hybrid	480	0.0066 m	6883 (-)	134.3 sec	6.7 sec	-18.6%
Hybrid	240	0.0066 m	6681 (-)	67.5 sec	3.4 sec	-19.0%
Hybrid	120	0.0066 m	6391 (-)	40.3 sec	2.0 sec	-28.7%
Hybrid*	120	0.0090 m	3079 (-)	20.3 sec	1.0 sec	-22.8%
Hybrid*	60	0.0090 m	2548 (-)	12.0 sec	0.6 sec	-31.2%
Hybrid*	60	0.0120 m	1582 (-)	8.0 sec	0.4 sec	-21.7%

- [10] K. Kamrin. Non-locality in granular flow: phenomenology and modeling approaches. *Front. Phys.*, 7, 2019.
- [11] C. Coetzee. Discrete and continuum modelling of soil cutting. *Comp. Part. Mech.*, 2014.
- [12] S. Dunatunga and K. Kamrin. Continuum modeling and simulation of granular flows through their many phases. *J. Fluid Mech*, 2015.
- [13] G. Tardos, S. McNamara, and I. Talu. Slow and intermediate flow of a frictional bulk powder in the couette geometry. *Powder Technology*, 131:23–39, 2003.
- [14] E. McKyes. Soil cutting and tillage. 1985.
- [15] D. Holz, A. Azimi, M. Teichmann, and S. Mercier. Real-time simulation of mining and earthmoving operations: a level set-based model for tool-induced terrain deformations. *30th International Symposium on Automation and Robotics in Construction and Mining (ISARC)*, 2013.
- [16] A. Reece. The fundamental equation of earth-moving mechanics. *Proceedings of the Institution of Mechanical Engineers*, 1964.
- [17] K. Skonieczny. Modeling the effects of surcharge accumulation on terrestrial and planetary wide-blade soil–tillage tool interactions. *Soil and Tillage Research*, 2018.
- [18] M. Muller, B. Heidelberger, M. Hennix, and Ratcliff J. Position based dynamics. *Journal of Engineering Mechanics*, 2006.
- [19] D. Holz. Parallel particles: a parallel position based approach for fast and stable simulation of granular materials. *Workshop on Virtual Reality Interaction and Physical Simulation VRIPHYS*, 2014.
- [20] E. Karpman, D. Holz, J. Kovacs, P. Niksirat, and K. Skonieczny. Particle-based modelling for wheel-soil interaction and analysis of effects of gravity. *International Conference On Particle-Based Methods. Fundamentals and Applications*, 2019.
- [21] Y. Hu, Y. Fang, Z. Ge, Z. Qu, Y. Zhu, A. Pradhana, and C. Jiang. A moving least squares material point method with displacement discontinuity and two-way rigid body coupling. *ACM Transactions on Graphics (TOG)*, 37(4):150, 2018.
- [22] C. Jiang, C. Schroeder, A. Selle, J. Teran, and A. Stomakhin. The affine particle-in-cell method. *ACM Transactions on Graphics*, 34(51), 2015.
- [23] David L. Henann and Ken Kamrin. Continuum thermomechanics of the nonlocal granular rheology. *International Journal of Plasticity*, 60:145–162, 2014.
- [24] S. Dunatunga. *A framework for continuum simulation of granular flow*. PhD dissertation, Massachusetts Institute of Technology, 2017.
- [25] D. Henann and K. Kamrin. A finite element implementation of the nonlocal granular rheology. *International Journal for Numerical Methods in Engineering*, 60, 2016.
- [26] D. Holz and A. Galarneau. Real-time mud simulation for virtual environments. In *ACM SIGGRAPH Symposium on Interactive 3D Graphics and Games (i3D)*, 2018.
- [27] H. Oraveca, X. Zenga, and V. Asnanib. Design and characterization of grc-1: A soil for lunar terramechanics testing in earth-ambient conditions. *Journal of Terramechanics*, 2010.
- [28] D. Jud, G. Hottiger, P. Leemann, and M. Hutter. Planning and control for autonomous excavation. *IEEE Robotics and Automation Letters*, 2(4):2151–2158, 2017.